

NIH RELAIS Document Delivery

NIH-10286761

JEFFDUYN

NIH -- W1 J0595L

JOZEF DUYN
10 Center Dirve
Bldg. 10/Rm.1L07
Bethesda, MD 20892-1150

ATTN: SUBMITTED: 2002-08-29 17:22:18
PHONE: 301-594-7305 PRINTED: 2002-09-03 06:16:53
FAX: - REQUEST NO.: NIH-10286761
E-MAIL: SENT VIA: LOAN DOC
7967423

NIH	Fiche to Paper	Journal
TITLE:	JOURNAL OF COMPUTER ASSISTED TOMOGRAPHY	
PUBLISHER/PLACE:	Lippincott Williams & Wilkins, Hagerstown, MD :	
VOLUME/ISSUE/PAGES:	1994 Sep-Oct;18(5):680-7	680-7
DATE:	1994	
AUTHOR OF ARTICLE:	Duyn JH; van Gelderen P; Barker P; Frank JA; Mattay VS; Moon	
TITLE OF ARTICLE:	3D bolus tracking with frequency-shifted BURST MRI	
ISSN:	0363-8715	
OTHER NOS/LETTERS:	Library reports holding volume or year 7703942 8089313	
SOURCE:	PubMed	
CALL NUMBER:	W1 J0595L	
REQUESTER INFO:	JEFFDUYN	
DELIVERY:	E-mail: jhd@helix.nih.gov	
REPLY:	Mail:	

NOTICE: THIS MATERIAL MAY BE PROTECTED BY COPYRIGHT LAW (TITLE 17, U.S. CODE)

----National-Institutes-of-Health,-Bethesda,-MD-----

3D Bolus Tracking with Frequency-Shifted BURST MRI

Jeff H. Duyn, Peter van Gelderen, Peter Barker, Joseph A. Frank, Venkata S. Mattay,
and Chrit T. W. Moonen

Objective: Our goal was to develop and test a 3D bolus-tracking MR technique for perfusion imaging of normal and pathological (infarcted) human brain.

Materials and Methods: All experiments were performed on standard 1.5 T GE/Signa clinical scanners. Five normal volunteers and one patient with a subacute brain infarct were studied. Modified [frequency-shifted (FS)] BURST MRI was performed during injection of a bolus of Gd-DTPA (0.13 mmol/kg) in the antecubital vein. The 3D datasets were acquired with a time resolution of 2.2 s and an effective spatial resolution of $4.3 \times 4.3 \times 6.4$ mm. Three-dimensional maps of blood volume and bolus arrival time were determined by fitting a synthetic curve to the intensity time course on a voxel-by-voxel basis.

Results: Both relative cerebral blood volume and arrival time maps demonstrated sensitivity to regional differences in blood supply in both normal brain and in the subacute brain infarction. The transit time maps showed arrival time delays of 5–7 s within and around the infarct and confirmed the diagnosis of left middle cerebral artery occlusion.

Conclusion: The results of the measurements on both normal and diseased human brain demonstrated the ability to acquire valuable 3D information about brain perfusion using FS BURST MRI.

Index Terms: Brain—Brain, perfusion—Magnetic resonance imaging, techniques—Arteries, occlusion.

The measurement of cerebral perfusion is an important element in the study of both normal and impaired human brain function. The connection between brain activity and perfusion has been well established (1–4). Altered perfusion has been observed in several diseases, including brain infarction (5–7), tumors (8,9), and neurodegenerative disorders (10,11). Among the techniques used to study perfusion are PET (12,13), Xe-CT (14), SPECT (15), and MRI (16–18).

Several researchers have studied brain perfusion

by dynamic MRI using an intravenous bolus administration of a contrast agent in both humans (19–21) and animal models (22,23). These methods are based on the susceptibility-induced signal losses upon the passage of the contrast agent through the microvasculature. Although these methods do not measure perfusion (or cerebral blood flow) in classical units (24), they allow for evaluation of the related (25,26) variable relative cerebral blood volume (rCBV). Since the transit time through the brain is only on the order of a few seconds (27,28), fast T_2^* -sensitized MRI techniques are required, such as EPI (29), FLASH (30), or ES-FLASH (31), or their segmented versions (32,33). Due to the time constraint, only single slices have been studied with FLASH or ES-FLASH. This is a severe limitation since, in many pathologies, the area of interest is not a priori known or extends over multiple slices. The EPI technique allows multislice imaging within a few seconds, but needs dedicated hardware.

Recently, a fast 3D T_2^* -sensitized imaging method, called frequency-shifted (FS) BURST (34), was introduced. This method allows for scanning of the whole brain within a few seconds. For bolus

From the Laboratory of Diagnostic Radiology Research, OIR (J. H. Duyn, J. A. Frank, and V. S. Mattay), In Vivo NMR Research Center, BEIP, NCRR (P. van Gelderen and C. T. W. Moonen), and Clinical Brain Disorders Branch, NIMH (V. S. Mattay and C. T. W. Moonen), National Institutes of Health, Bethesda, and Johns Hopkins Medical Institutions, Baltimore (P. Barker), Maryland, U.S.A. Address correspondence and reprint requests to Dr. J. H. Duyn at Laboratory of Diagnostic Radiology Research, OIR, Bldg. 10, Rm. B1N-256, National Institutes of Health, Bethesda, MD 20892, U.S.A.

Work of the U.S. government. Not subject to copyright in the United States.

tracking, the attractive feature of this method is the fact that it has, unlike EPI and segmented FLASH, equal $T2^*$ weighting over k -space lines. Here we will discuss the application of this method to MR perfusion imaging.

MATERIALS AND METHODS

All experiments were performed on standard 1.5 T GE Signa clinical scanners (GE Medical Systems, Milwaukee, WI, U.S.A.), equipped with 10 mT/m, actively shielded whole-body gradients. A standard quadrature head RF coil was used. Five normal volunteers and one patient with a subacute brain infarct were studied. The subject with acute infarction, a 39-year-old woman and intravenous drug user, was diagnosed with a left middle cerebral artery occlusion and was scanned 3 days postictus. The human subject protocols were approved by the intramural review board of the National Institutes of Health and the Joint Committee for Clinical Investigation of the Johns Hopkins School of Medicine.

The MR method used for 3D bolus tracking was based on FS BURST as described in ref. 34. The essentials of this method can be summarized as follows: Excitation of magnetization is performed by a BURST pulse (35), which consists of a train of evenly spaced, low flip angle RF pulses in combination with a slice select gradient. Multiple trains of measurable echo signals can be generated by repeated reversal of the selection gradient (Fig. 1). By applying a second switched gradient (PE-1 in Fig. 1), a second dimension of spatial encoding is incorporated in each echo train, allowing scanning of a complete image plane within a single repetition of

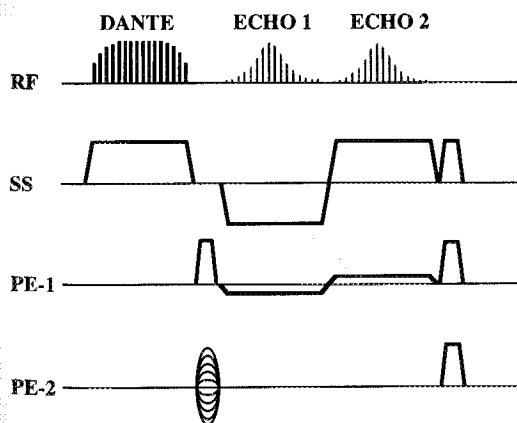


FIG. 1. 3D FS BURST pulse sequence. The excitation consists of a Hamming-apodized BURST RF pulse in combination with a slice selection (SS) gradient. Two echo trains (ECHO 1, ECHO 2) are created by repeated gradient reversal. The echo trains are phase encoded in two directions by PE-1 and PE-2. A gradient crusher is applied after collection of the second echo.

the sequence. The addition of a third gradient (PE-2), the amplitude of which is varied over subsequent repetitions of the sequence, allows scanning of 3D volumes. Saturation effects were avoided by applying a frequency shift to the RF pulse on successive repetitions (34).

For 3D bolus tracking, the original sequence was modified on the following points:

1. Instead of acquiring two echo trains, only the second echo train was collected. It has been shown (34) that, in contrast with the first echo train, the second echo train has an inherent uniform $T2^*$ weighting. This allows for susceptibility-weighted scanning without image artifacts.

2. A reduction of the scan time was established by reducing the number of sample points and the size of the FOV.

3. The effective TE of the second echo train was reduced to improve contrast-to-noise ratio.

Furthermore, of the two FS protocols presented previously (34), the single-strip shift protocol was chosen.

The BURST RF pulse consisted of a train of 48 evenly spaced pulses. The pulse spacing was 288 μ s, the total BURST pulse length 13.7 ms. The individual RF pulses were 128 μ s long, and were apodized with a combination of a sinc and a Gaussian function. In combination with selection gradients, applied simultaneously in anteroposterior and superoinferior directions, this resulted in selection of a 150 mm thick slab with $\sim 45^\circ$ angulation (see Fig. 3 for example). The specific angle was used to utilize the maximum effective gradient strength to achieve optimum resolution. An echo train of 40 echoes was acquired with an effective TE of 28.8 ms. The reason for acquiring less echoes than the number of BURST RF pulses was to reduce the TR without affecting the selection properties of the BURST pulse. Each echo contained 36 data points and 48 phase-encoded repetitions were performed using TR = 45 ms. A $36 \times 40 \times 48$ data matrix was collected using a $22 \times 16 \times 19.2$ cm FOV. The measurement time was 2.16 s with 30–40 scans recorded sequentially, resulting in a total measurement time of 65–87 s. The prolonged use of strong gradients did not result in excessive heating of the gradient coils.

For comparison and on the normal subjects only, 2D FLASH dynamic imaging was performed with TE/TR = 27/33.8 and a 128×64 data matrix. This resulted in a scan time of 2.16 s, equivalent to that of the 3D experiment. Between the 3D and 2D experiments, a delay of at least 30 min was used.

Ten seconds after the start of each dynamic imaging experiment, a bolus of Gd-DTPA solution was administered at a rate of 6 ml/s using a mechanical injector (Medrad, Pittsburgh, PA, U.S.A.) through an 18 gauge catheter placed in the antecubital vein. A dose of 0.13 mmol/kg body wt was used, resulting

in injection times of 3–5 s (typical). For the stroke patient, a 0.15 mmol/kg dose was hand injected within 6–10 s.

Data processing was performed off-line using Sun-SPARC 10 workstations (Sun Microsystems, Mountainview, CA, U.S.A.) with IDL processing software (Research Systems, Boulder, CO, U.S.A.). Prior to the 3D Fourier transformation, a 20% Hamming filter was applied over each echo and over the second phase encode dimension. Also before Fourier transformation, the dataset was zero-filled to a $64 \times 64 \times 64$ matrix. The effective resolution was $6.4 \times 4.3 \times 4.3$ mm. Magnitude images were then used to calculate the rCBV maps. Also calculated were maps displaying the arrival time of the bolus, referred to here as "arrival time" maps. The calculations were performed by least-squares fitting of a synthetic curve to the time curve of each pixel inside the brain. Several types of synthetic curves, among which a gamma-variate function (36), were tested. The latter is a four parameter curve that, in cases of limited signal-to-noise ratio (SNR) and limited resolution, does not provide reliable fitting (37). For the specific SNR and time resolution of our data, a three parameter curve of the form

$$f(t) = a - b \left\{ e^{-(t+c)/w} + 0.15 \left[\frac{\pi}{2} + \arctan \left(\frac{1.33(t+c)}{w} \right) \right] - 0.042(t+c+1) \right\}$$

with $t = \text{time} [-1, \dots, 1]$, $a = \text{prebolus signal level (variable)}$, $b = \text{bolus intensity (variable)}$, $c = \text{bolus arrival time (variable)}$, and $w = \text{width of bolus passage (fixed)}$ was used. The exponential term of the function describes a Gaussian time course of signal loss during the bolus passage, whereas the arc-tangent and constant slope terms account for persistent signal loss after passage of the bolus. The function resulted in almost all (>95%) of the pixels in a convergent fit and gave a fairly accurate representation of the signal loss during and after the passage of the bolus. The function was based on the following assumptions: a quasicontant prebolus signal level (a), a quasicontant postbolus signal loss related to the bolus intensity proportional to bolus intensity (b), and a variable bolus arrival time (c). Monte Carlo simulations were performed to determine the propagation of measurement noise into noise in the fitted parameters. Furthermore, to check accuracy of the fitting procedure with respect to systematic errors, maps of the sum of squared differences between time course data and fit results were created and normalized to baseline signal intensity (a). The total computation time for Fourier transformation and time curve fitting was ~ 25 min.

After time curve fitting, the rCBV maps were calculated from $\text{rCBV} = \ln(b/a)$ (20). Arrival time maps were calculated from c and thresholded with parameter b (pixels with a b value less than a fifth of the average gray matter value were set to background intensity level).

RESULTS AND DISCUSSION

All 3D FS BURST measurements demonstrated an SNR of ~ 30 and a stability of 20 (both numbers based on standard deviations). In the studies on normal subjects, the maximum signal loss during bolus passage was 30–50% for normal gray matter pixels. The study on brain infarction showed a lower bolus intensity (20–35%), possibly due to the lower injection rate. An example of a typical fit in a gray matter pixel of normal brain is shown in Fig. 2. The Monte Carlo simulations, based on this fit and assuming SNR = 20, resulted in estimated standard deviations for baseline signal level, rCBV, and arrival time of 1.5%, 8.0%, and 0.45 s, respectively. Errors in actual perfusion measurements may be larger, since no systematic errors were included in this analysis, and both SNR and/or bolus intensity are much reduced in certain brain areas (e.g., white matter).

Figure 3 shows an example of the calculated rCBV maps from a normal subject: Displayed are images from a section of 24 slices, covering about two-thirds of the brain. As expected, gray matter areas appear bright in the images, indicating a relatively high blood volume. Clearly identifiable are also the ventricular system, the sylvian fissures, and the tentorium. As evident from the illustrative material of several other reports on the subject, on the rCBV maps, part of the ventricular system appears bright. A possible explanation is the signal

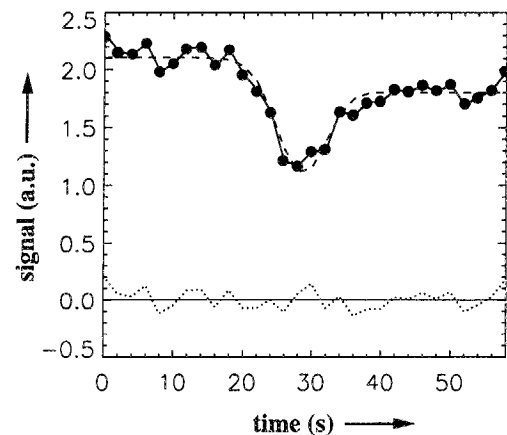
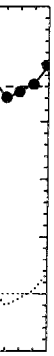


FIG. 2. Typical time course data from a gray matter pixel of normal brain. Pixel intensity is given as a function of time (dots connected with solid line), together with the fitted time curve (dashed line) and the fit residuals (dotted line).

os were cal-
 arrival time
 oided with
 an a fifth of
 et to back-

monstrated
 h numbers
 studies on
 oss during
 ray matter
 showed a
 due to the
 ical fit in a
 n in Fig. 2.
 this fit and
 d standard
 V, and ar-
 spectively.
 ts may be
 ncluded in
 s intensity
 e.g., white

calculated
 played are
 ring about
 ray matter
 ating a re-
 ifiable are
 n fissures,
 llustrative
 ument, on
 ystem ap-
 the signal



ter pixel of
 ion of time
 e fitted time
 ine).

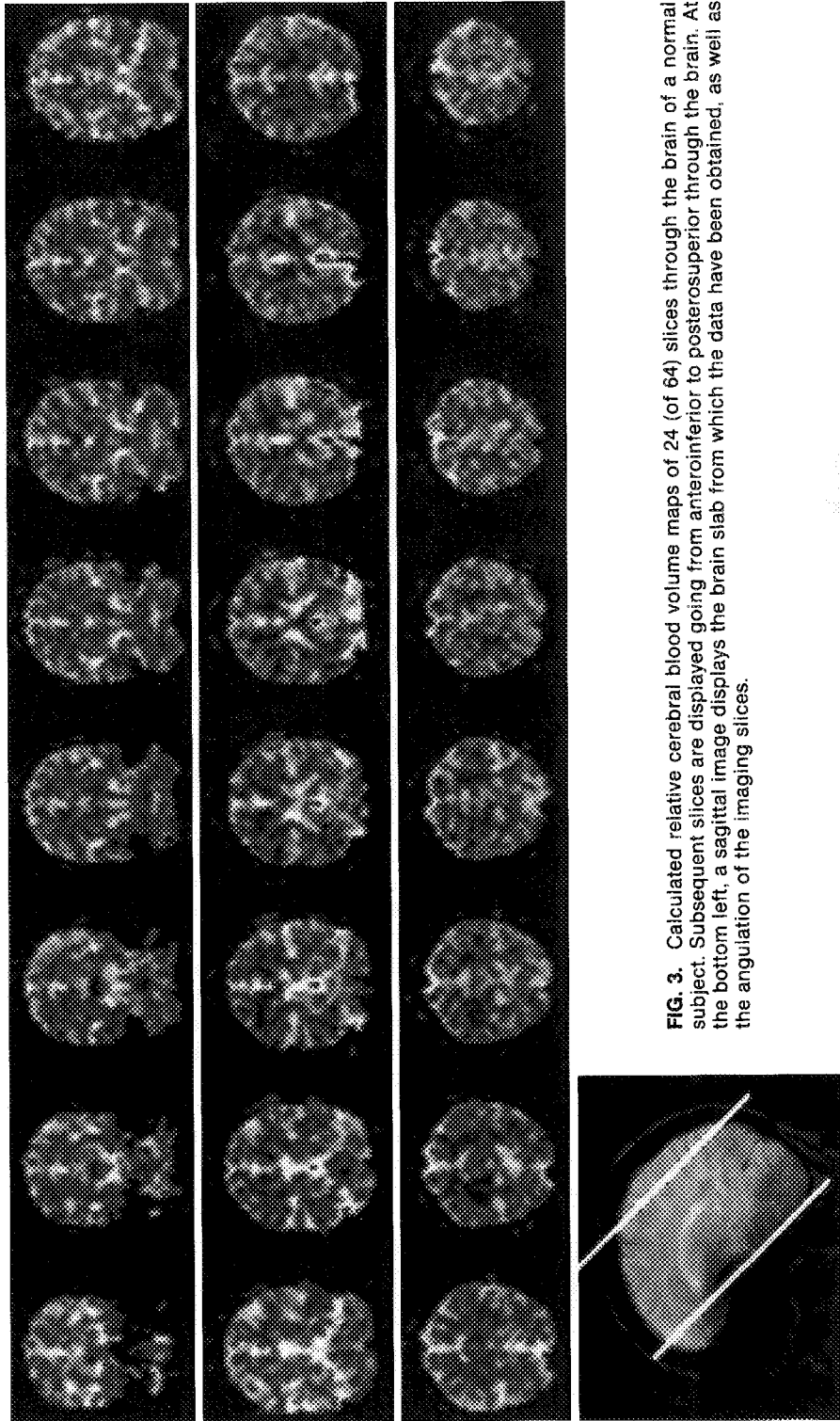


FIG. 3. Calculated relative cerebral blood volume maps of 24 (of 64) slices through the brain of a normal subject. Subsequent slices are displayed going from anterior to posterior through the brain. At the bottom left, a sagittal image displays the brain slab from which the data have been obtained, as well as the angulation of the imaging slices.

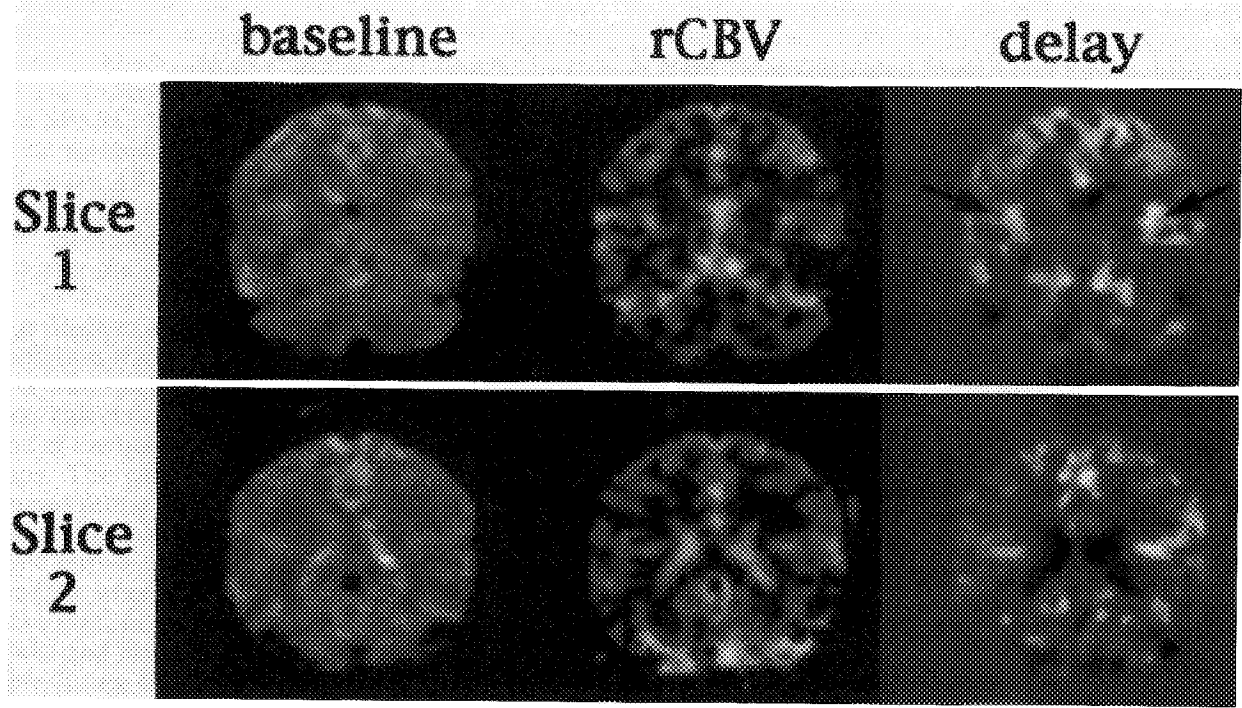


FIG. 4. Calculated baseline intensity, relative cerebral blood volume (rCBV), and arrival time maps in two slices of the dataset from Fig. 3. The gray scale in the arrival time maps runs from early (white) to late arrival (black) and spans 4 s. Note the early bolus arrival around the larger arteries, especially the middle cerebral arteries in slice 1 (insular arteries indicated with arrows). Notice the late signal shift (bright to dark) in the ventricular system, as well as the late arrival in the large vessels (veins?) in the posterior brain.

loss due to macroscopic susceptibility effects during bolus passage through the larger vessels bordering the ventricles.

Two slices of this dataset are shown enlarged in Fig. 4, together with corresponding baseline signal and arrival time maps. Most striking of this figure are the arrival time (delay) maps, which indicate early arrival of the contrast agent bolus in the major cerebral arteries (anterior, middle, and posterior) and surrounding regions. Also striking is the late (delay = 2–4 s) shift in signal (from bright to dark) of the ventricular system as well as the late arrival in the larger vessels, including sinuses, of the posterior brain.

In Fig. 5, a comparison is shown between an rCBV map, obtained with FLASH, and a slice of the 3D FS BURST rCBV dataset. Although the

FLASH rCBV map exhibits superior resolution, general features are quite similarly represented with both methods. Figure 5c shows a map of the normalized sum of squared differences between time data and fit of the FS BURST data. The map is relatively uniform, i.e., shows only faintly recognizable structure, indicating minimal systematic fit errors. Most of the remaining structure is caused by differences in baseline signal intensity.

The results of the measurements of subacute brain infarction are shown in Figs. 6 and 7. The SNR of the FS BURST data was somewhat inferior to that in the studies on the normal subjects. This is partly attributed to the use of a hand-performed bolus administration as opposed to use of a mechanical injector. The T2-weighted MRI (TE/TR = 80/3,000 ms) showed hyperintense regions in the in-

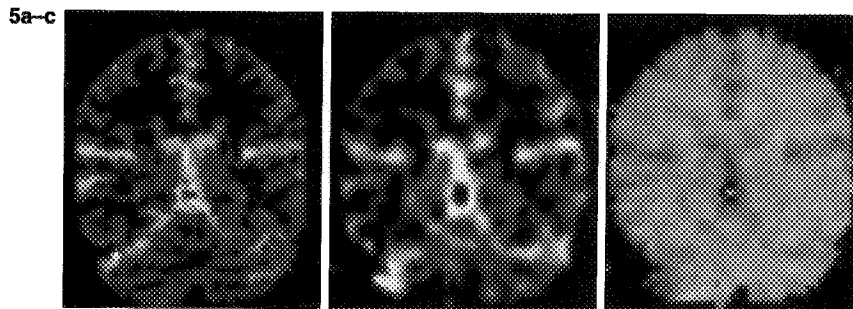


FIG. 5. Calculated rCBV maps from 2D FLASH (a) and FS BURST (b), obtained from similar sections of normal brain. Although the FLASH relative cerebral blood volume map shows finer detail, the appearance of larger structures is similar with both FLASH and FS BURST. In (c) a normalized map of the sum of squared differences between time course data and fit results is displayed. Its intensity is fairly uniform, indicating only minor contribution of systematic errors to the fit results.

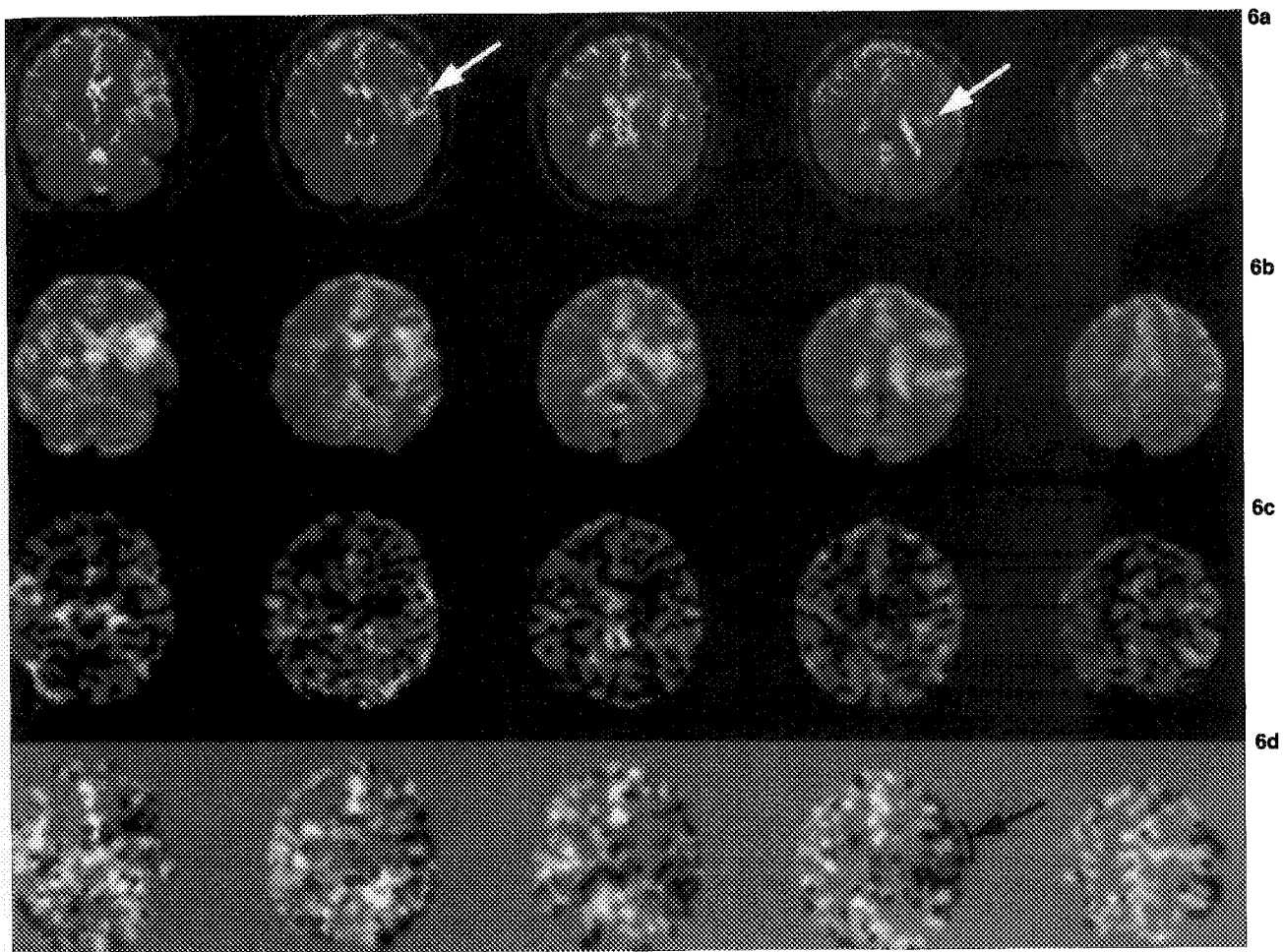


FIG. 6. T2-weighted MRI (a) and 3D FS BURST perfusion measurement (b-d) of subacute brain infarction. Five slices (every third slice from a 3D dataset) are displayed going from inferoanterior to superoposterior through the brain. Slice numbers are indicated at the top of the figure. Each of the rows shows T2-weighted data (a), calculated baseline intensity (b), relative cerebral blood volume (c), and arrival time (d). The location of the infarct is indicated with the white arrows in (a), whereas part of the affected region from which time course data were examined is indicated with the black arrow in (d). The spread in arrival time in (d) is 7-8 s.

infarcted hemisphere (Fig. 6a). Signal baseline level, rCBV, and arrival time maps were calculated from the FS BURST data and are shown in Fig. 6b, c, and d, respectively. The baseline images (Fig. 6b) show hyperintensities similar to those observed in the T2-weighted data. Some signal loss is observed in the rCBV maps (Fig. 6c) at the site of the stroke, whereas some peripheral areas (especially in slices 34 and 37) show increased rCBV. Again, the most striking changes were seen in the arrival time maps. Regions surrounding the hyperintense areas in the T2-weighted maps appear dark, indicating late arrival of the bolus. The latter finding is consistent with the presence of "luxury perfusion" (38). Signal time course data from a pixel within the infarcted area (white arrow in Fig. 6), from 2 pixels adjacent to the infarct (black arrow in Fig. 6), and from a contralateral normal-appearing area are shown in Fig. 7 a-d. Although most pixels adjacent to the infarcted region show a arrival time delay of 5-7 s,

significant areas remain with a normal or only a partially delayed bolus arrival time.

CONCLUSIONS

The results of the measurements on both normal and diseased human brain demonstrated the ability to acquire 3D information about brain perfusion using FS BURST MRI. Comparison with conventional 2D FLASH bolus tracking showed that similar rCBV maps can be obtained with both methods, although the finest details seen in the 2D method are largely lost with 3D FS BURST, due to the reduced spatial resolution. The gain with 3D FS BURST lies in its ability to obtain a complete, qualitative picture of perfusion, without restricting the view to a single brain slice. This can be of paramount importance in studies of lesions of extensive size or uncertain location. The presented measurement on brain infarct-

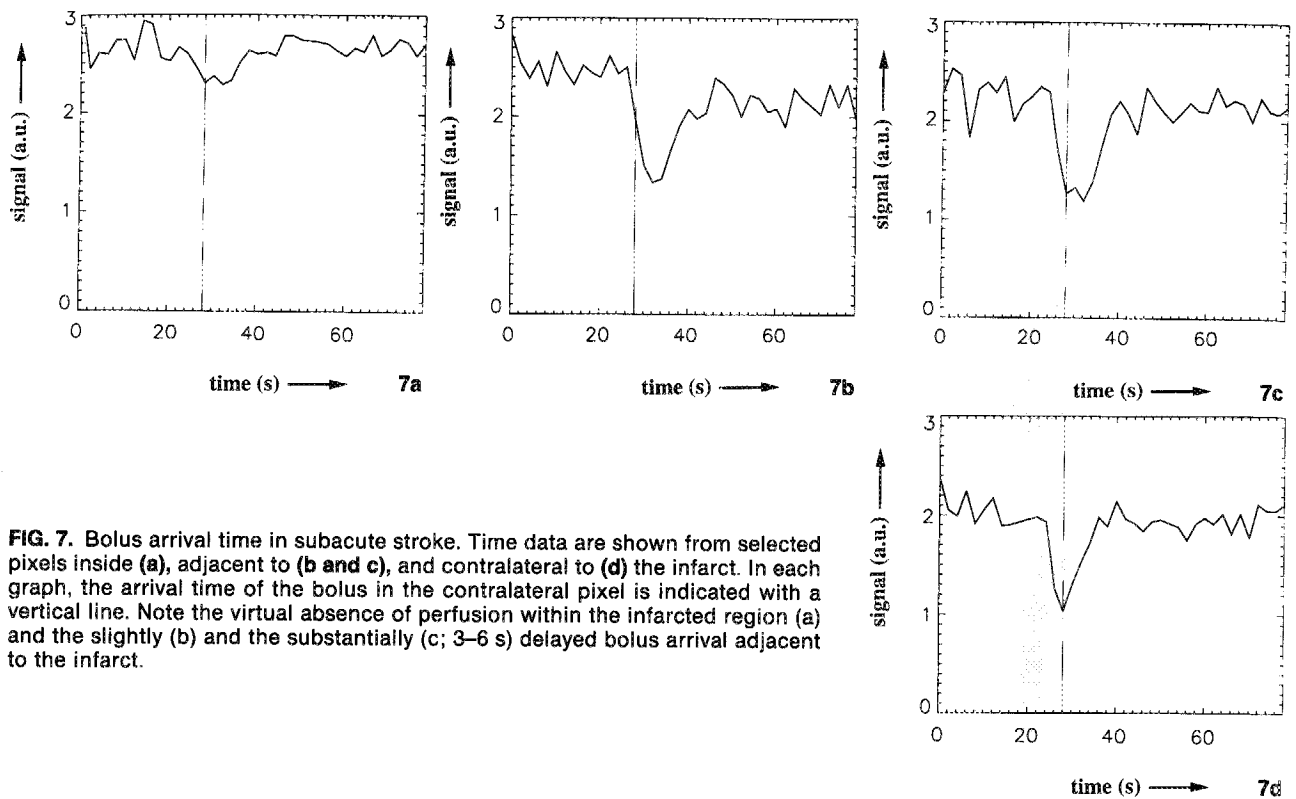


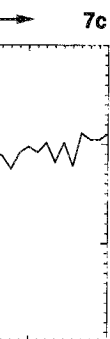
FIG. 7. Bolus arrival time in subacute stroke. Time data are shown from selected pixels inside (a), adjacent to (b and c), and contralateral to (d) the infarct. In each graph, the arrival time of the bolus in the contralateral pixel is indicated with a vertical line. Note the virtual absence of perfusion within the infarcted region (a) and the slightly (b) and the substantially (c; 3–6 s) delayed bolus arrival adjacent to the infarct.

tion, showing regional variability of both rCBV and bolus arrival time in areas within and around the infarcted region, stresses this point.

Acknowledgment: P. Barker was supported in part by the Whitaker Foundation, Mechanicsburg, PA. Drs. P. van Zijl, R. S. Sexton, F. Barrios, G. S. Sobering, K. Kotrla, D. Weinberger, J. Black, and R. Hill are gratefully acknowledged for their support and/or helpful suggestions.

REFERENCES

- Roy CS, Sherrington CS. On the regulation of the blood supply of the brain. *J Physiol (Lond)* 1890;11:85–108.
- Ter-Pergossian MM, Herscovitch P. Radioactive oxygen-15 in the study of cerebral blood flow, blood volume, and oxygen metabolism. *Semin Nucl Med* 1985;15:377–94.
- Raichle ME. In: Shepherd JT, Abboud FM, eds. *Handbook of physiology. The nervous system 5*. Bethesda: American Physiology Society, 1987:643–674.
- Sokoloff L. Relationships among local functional activity energy metabolism and blood flow in the central nervous system. *Fed Proc* 1981;40:2311–6.
- Seiderer M, Krappel W, Moser E, et al. Detection and quantification of chronic cerebrovascular disease: comparison of MR imaging, SPECT, and CT. *Radiology* 1989;170:545–48.
- Edelman RR, Mattle HP, Atkinson DJ, et al. Cerebral blood flow: Assessment with dynamic contrast-enhanced T2*-weighted MR imaging at 1.5 T. *Radiology* 1990;176:211–20.
- Tzika AA, Massoth RJ, Ball WS, et al. Cerebral perfusion in children: detection with dynamic contrast-enhanced T2*-weighted MR images. *Radiology* 1993;187:449–58.
- Di Chiro G, Oldfield E, Wright DC, et al. Cerebral necrosis after radiotherapy and/or intraarterial chemotherapy for brain tumors: PET and neuropathologic studies. *AJR* 1988; 150:189–97.
- Rosen BR, Belliveau JW, Aronen HJ, et al. Susceptibility contrast imaging of cerebral blood volume: human experience. *Magn Res Med* 1991;22:293–9.
- Andreasen NC. Brain imaging: applications in psychiatry. *Science* 1988;239:1381–8.
- DeKosky ST, Shih W-J, Schmitt FA, Coupal J, Kirkpatrick C. Assessing utility of single photon emission computed tomography (SPECT) scan in Alzheimer's disease: correlation with cognitive study. *Alzheimers Dis Assoc Disord* 1990;4: 14–23.
- Herscovitch P, Markham J, Raichle ME. Brain blood flow measurement with intravenous H₂¹⁵O. 1: theory and error analysis. *J Nucl Med* 1984;24:782–9.
- Baron JC, Frackowiak RSJ, Herholz K, et al. Use of PET methods for measurement of cerebral energy metabolism and hemodynamics in cerebrovascular disease. *J Cereb Blood Flow Metab* 1989;9:723.
- Gur D, Good WF, Wolfson SK, Yonas H, Shabson L. In vivo mapping of local cerebral blood flow by xenon-enhanced computed tomography. *Science* 1982;215:1267–8.
- Celsius P, Goldman T, Henriksen L, Lassen NA. A method for calculating regional cerebral blood flow from emission computed tomography of inert gas concentrations. *J Comput Assist Tomogr* 1981;5:641–5.
- Williams DS, Detre JA, Leigh JS, Koretsky AP. Magnetic resonance imaging of perfusion using spin inversion of arterial water. *Proc Natl Acad Sci USA* 1992;89:212–6.
- Ackerman JJH, Ewy CS, Becker NN, Schwalz RA. Deuterium nuclear magnetic resonance of blood flow and tissue perfusion employing ²H₂O as a freely diffusible tracer. *Proc Natl Acad Sci USA* 1987;84:4099–102.
- Barranco D, Sutton LN, Florin S, et al. Use of ¹⁹F NMR spectroscopy for measurement of cerebral blood flow: a comparative study using microspheres. *J Cereb Blood Flow Metab* 1989;9:886–91.



19. Villringer A, Rosen BR, Belliveau JW, et al. Dynamic imaging with lanthanide chelates in normal brain: contrast due to magnetic susceptibility effects. *Magn Res Med* 1988;6:164-74.
20. Rosen BR, Belliveau JW, Vevea JM, Brady TJ. Perfusion imaging with NMR contrast agents. *Magn Res Med* 1990;14:249-65.
21. Belliveau JW, Kennedy DN, McKinstry RC, et al. Functional mapping of the human visual cortex by magnetic resonance imaging. *Science* 1990;254:716.
22. Kucharczyk J, Vexler ZS, Roberts TP, et al. Echo-planar perfusion-sensitive MR imaging of acute cerebral ischemia. *Radiology* 1993;188:711-7.
23. Moseley ME, de Crespigny AJ, Roberts TP, Kozniwska E, Kucharczyk J. Early detection of regional cerebral ischemia using high-speed MRI. *Stroke* 1993;24 (suppl 12):160-5.
24. Weisskoff RM, Chesler D, Boxerman JL, Rosen BR. Pitfalls in MR measurements of tissue blood flow with intravascular tracers: which mean transit time? *Magn Res Med* 1993;29:553-9.
25. Grubb RL, Raichle ME, Eichling JO, Ter-Pergossian MM. The effects of changes in PaCO₂ on cerebral blood volume, blood flow, and vascular mean transit time. *Stroke* 1974;5:630-9.
26. Smith AL, Neufeld GR, Ominsky AJ, Wollman H. Effect of arterial CO₂ tension on cerebral blood flow, mean transit time, and vascular volume. *J Appl Physiol* 1971;31:701-7.
27. Greitz T. Normal cerebral circulation time as determined by carotid angiography with sodium and methylglucamine diatrizoate (uragrafin). *Acta Radiol [Diagn] (Stockh)* 1968;7:331-6.
28. Axel L. Cerebral blood flow determination by rapid-sequence computed tomography. *Radiology* 1980;137:679-86.
29. Mansfield P, Pykett I. Biological and medical imaging by NMR. *J Magn Res* 1978;29:355-73.
30. Haase A, Frahm J, Matthai D, Haenicke W, Merboldt KD. FLASH imaging. Rapid NMR imaging using low flip-angle pulses. *J Magn Res* 1986;67:258-66.
31. Moonen CTW, Liu G, van Gelderen P, Sobering G. Fast echo-shifted gradient-recalled MRI: combining a short repetition time with a variable T2* weighting. *Magn Res Med* 1992;26:184-9.
32. McKinnon GC. Ultrafast interleaved gradient-echo-planar imaging on a standard scanner. *Magn Res Med* 1993;30:609-16.
33. Liu G, Sobering G, Duyn JH, Moonen CTW. A functional MRI technique combining principles of echo-shifting with a train of observations (PRESTO). *Magn Res Med* 1993;30:764-8.
34. Duyn JH, van Gelderen P, Liu G, Moonen CTW. Fast volume scanning with frequency-shifted BURST MRI. *Magn Res Med* (in press).
35. Hennig J, Hoddap M. Burst imaging. *MAGMA* 1993;1:39-48.
36. Thompson HK, Starmer CF, Whalen RE, McIntosh HD. Indicator transit time considered as a gamma variate. *Circ Res* 1964;14:502-14.
37. Lu D, Monahan WG. Effect of sample numbers on the kinetic data analysis of MR contrast agents. *Magn Res Med* 1993;30:131-4.
38. Lassen NA. The luxury-perfusion syndrome and its possible relation to acute metabolic acidosis within the brain. *Lancet* 1966;2:1113-5.

AJR 1988;

sceptibility
man experi-

psychiatry.

Kirkpatrick
omputed to-
correlation
ord 1990;4:

blood flow
and error

Use of PET
metabolism
e. *J Cereb*

bson L. In
by xenon-
15:1267-8.
A method
n emission
J Comput

. Magnetic
ion of arte-
-6.

RA. Deu-
and tissue
racer. *Proc*

¹⁹F NMR
od flow: a
blood Flow